

## On the nature of rotation in the Praesepe cluster

C. J. HAO,<sup>1,2</sup> Y. XU,<sup>1,2</sup> S. B. BIAN,<sup>1,2</sup> L. G. HOU,<sup>3</sup> Z. H. LIN,<sup>1,2</sup> Y. J. LI,<sup>1</sup> AND D. J. LIU<sup>1,2</sup>

<sup>1</sup>*Purple Mountain Observatory, Chinese Academy of Sciences, Nanjing 210023, PR China*

<sup>2</sup>*School of Astronomy and Space Science, University of Science and Technology of China, Hefei 230026, PR China*

<sup>3</sup>*National Astronomical Observatories, Chinese Academy of Sciences, 20A Datun Road, Chaoyang District, Beijing 100101, PR China*

### ABSTRACT

Although a large number of Galactic open clusters (OCs) have been identified, the internal kinematic properties (e.g., rotation) of almost all the known OCs are still far from clear. With the high-precision astrometric data of *Gaia* EDR3, we have developed a methodology to unveil the rotational properties of the Praesepe cluster. Statistics of the three-dimensional residual motions of the member stars reveal the presence of Praesepe’s rotation and determine its spatial rotation axis. The mean rotation velocity of the Praesepe cluster within its tidal radius is estimated to be  $0.2 \pm 0.05 \text{ km s}^{-1}$ , and the corresponding rotation axis is tilted in relation to the Galactic plane with an angle of  $41^\circ \pm 12^\circ$ . We also analysed the rms rotational velocity of the member stars around the rotation axis, and found that the rotation of the member stars within the tidal radius of Praesepe probably follows the Newton’s classical theorems.

**Keywords:** open clusters and associations: individual (Praesepe) – stars: kinematics and dynamics – methods: statistical

### 1. INTRODUCTION

The open star clusters in the Galaxy are gravitationally bound systems, and present a wide range of ages from a few million years to several billion years. An open cluster (OC) typically contains tens to thousands of member stars, which formed almost simultaneously in the same molecular cloud (e.g., Lada & Lada 2003). OCs serve as excellent astronomical laboratories for studying the stellar structure and evolution (e.g., Barnes 2007; Bertelli Motta et al. 2017; Marino et al. 2018), and are good tracers for unveiling the structure and evolution of our Galaxy (Castro-Ginard et al. 2021; Poggio et al. 2021; Hao et al. 2021; Hou 2021). Although thousands of OCs have been identified in the Milky Way (Dias et al. 2002; Kharchenko et al. 2013; Cantat-Gaudin et al. 2020; Castro-Ginard et al. 2020; Hao et al. 2022; Castro-Ginard et al. 2022), little is known about their internal kinematics, such as rotation and whether they are expanding or contracting. These kinematic properties are strongly related to the formation and evolution of OCs.

In the early days, there were some efforts focused on investigating the effect of cluster rotation on the proper motion vector geometry of its member stars (e.g., Wayman 1967; Hanson 1975; Gunn et al. 1988; Perryman et al. 1998). Later, based on the dataset provided by the *Hipparcos* and WEBDA, Vereshchagin & Chupina (2013) and Vereshchagin et al. (2013) attempted to explore the potential rotation in the Hyades and Praesepe clusters. They found a correlation between the tangential velocities and the parallaxes of cluster members, which implies the possible rotation in the two OCs. Recently, by taking advantage of the released dataset of *Gaia* (Gaia Collaboration et al. 2016), some works studied the relationship between the tangential or radial velocities (RVs) and the angular radii for the member stars of some OCs (e.g., Kamann et al. 2019; Healy et al. 2021). The signals of rotation were found in the Praesepe and NGC 6791 clusters, but not for the Pleiades and NGC 6819 clusters. In brief, the kinematic properties have only been simply explored for several OCs, which remain as major omission in the studies of Galactic OCs.

In this study, we focus on the Praesepe cluster, also known as the Beehive Cluster, located at a distance of 170–190 pc from the Sun (e.g., Pinsonneault et al. 1998; Dias et al. 2002; Kharchenko et al. 2013; Cantat-

Gaudin et al. 2018; Gaia Collaboration et al. 2018a; Gao 2019). It is an intermediate-age cluster with an estimated age of 590–660 Myr (e.g., Mermilliod 1981; Vandenberg & Bridges 1984; Delorme et al. 2011; Brandt & Huang 2015; Gossage et al. 2018). The tidal radius of the Praesepe cluster is estimated to be in the range of [10, 12] pc (e.g., Adams et al. 2002; Khalaj & Baumgardt 2013; Lodieu et al. 2019; Röser & Schilbach 2019; Gao 2019; Loktin & Popov 2020). The member stars within the tidal radius of the cluster are generally gravitationally bound. As a rich OC, Praesepe contains red giants and white dwarfs representing the late stages of stellar evolution, as well as main-sequence stars and a significant number of low-mass stars (e.g., Dobbie et al. 2004, 2006; Kraus & Hillenbrand 2007; Wang et al. 2014; Gaia Collaboration et al. 2018a). Klein Wassink (1924, 1927) firstly studied this cluster. The low-mass members, binarity, luminosity and mass functions of the Praesepe cluster were then investigated by the subsequent works (see Lodieu et al. 2019, and references within). Recently, with the *Gaia* data, Röser & Schilbach (2019) found a clear indication for the existence of tidal tails in Praesepe, even stretching to about 165 pc from the cluster centre.

Based on the trigonometric parallaxes, proper motions, and RVs in *Gaia* data release 2 (DR2, Gaia Collaboration et al. 2018b), Loktin & Popov (2020) reported a possible rotation at the periphery of Praesepe with a velocity of  $0.4 \text{ km s}^{-1}$ . As the improved data quality of the *Gaia* early data release 3 (EDR3, Gaia Collaboration et al. 2021), the detailed kinematic properties are expected to unveil the nature of Praesepe further. In contrast to previous studies only using the projection methods, this study aims to investigate the global and particularly the internal kinematics of Praesepe in three dimensions (3D) simultaneously, according to the high-precision astrometric parameters of *Gaia* EDR3.

In this work, we will first extract the member stars of Praesepe from the *Gaia* EDR3, all of which have the six-parameter solutions and RVs. Subsequently, we develop a methodology used to study the kinematic properties of a Galactic OC, including calculating and analysing the 3D residual velocities of the member stars, determining the rotation axis if the cluster rotates, and deriving the rotational velocities of the member stars. This methodology is applied to the Praesepe cluster to characterize its kinematics.

## 2. SAMPLE OF THE MEMBER STARS

The member stars of Praesepe are relatively easy to identify, as the Praesepe cluster is close to the Sun and presents large proper motions (e.g., Pinsonneault et al.

1998; Dias et al. 2002; Kharchenko et al. 2013; Cantat-Gaudin et al. 2018; Gaia Collaboration et al. 2018a). To identify the possible members, we adopt a selection method similar to that of Loktin & Popov (2020), but based on the *Gaia* EDR3. First, the stars falling within a radius of  $10^\circ$  around the coordinates of *RA* (Right ascension) = 08h40m24s and *Dec* (Declination) =  $+19^\circ 40' 00''$  (J2000) are selected as the initial dataset. Field stars are then eliminated according to the diagram of trigonometric parallax ( $\varpi$ ) and apparent magnitude ( $G$ ). The selection boundary for the trigonometric parallax is set to [4.6, 6.1] mas, which represents three-times of the mean parallax uncertainty for the faint stars ( $G = 20$ ) in *Gaia* EDR3. A similar procedure is applied to the diagrams of proper motions ( $\mu_{\alpha^*}$ ,  $\mu_\delta$ ) and apparent magnitude, where the selection boundaries are set to be  $[-41, -31] \text{ mas yr}^{-1}$  and  $[-16, -10] \text{ mas yr}^{-1}$ , respectively, by referencing the mean and three-times standard deviation of  $\mu_{\alpha^*}$  and  $\mu_\delta$  reported by Loktin & Popov (2020). Similar to Loktin & Popov (2020, see their Figure 3), the stars below and far away from the main sequence are identified by eye and excluded according to a color-magnitude diagram, as indicated by the green dots in Figure 1(d), except for a group of white dwarfs already known to belong to Praesepe (e.g., Dobbie et al. 2004, 2006; Gaia Collaboration et al. 2018a). In addition, we notice that all the excluded objects are faint stars and do not possess RV measurements in *Gaia* EDR3. After eliminating the stars with uncertainties of trigonometric parallax or proper motions larger than 10%, we obtain a catalog containing 1 135 member stars. Figure 1 shows the distributions of the observed parameters (i.e., *RA*, *Dec*,  $\varpi$ ,  $\mu_{\alpha^*}$ , and  $\mu_\delta$ ) of the member stars, which are approximated by a multidimensional normal distribution. Objects that deviate from the three-times standard deviation of the mean values are possible field stars. We found that only about 5.8% of the member stars deviate in some of the five-dimensional space. The influence of contaminating field stars on the following results is believed to be small.

Because the aim of this study is to inspect the 3D kinematic properties of the Praesepe cluster, only the stars with RV measurements are extracted from the catalog. Here, we adopt only the RVs provided by *Gaia* to ensure the homogeneity of the sample and avoid the potentially significant systematic errors. Stars with uncertainties of RVs larger than  $2 \text{ km s}^{-1}$  are eliminated, in order to ensure an accurate measurements of RV. 20 outliers are further rejected after checking the member stars one by one, as they possess RV values that significantly diverge from the three-times standard deviation of the reported mean RV of Praesepe ( $35.1 \pm 1.6 \text{ km s}^{-1}$ , Loktin &

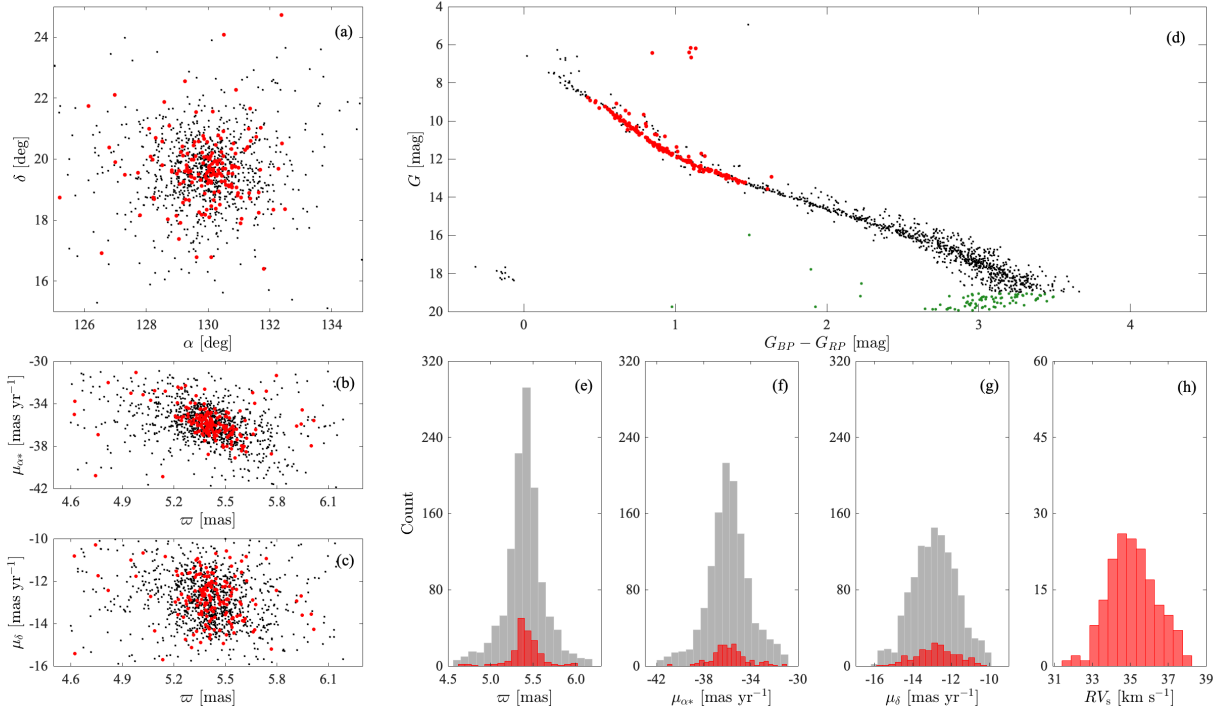


**Figure 1.** Properties of the parameters for the member stars (grey) of Praesepe, as well as those for the members with RV measurements (red). *Panel (a):* distribution on the sky. *Panels (b) and (c):* diagrams of parallax vs. proper motions. *Panel (d):* color–magnitude diagram, where the green dots represent the excluded stars that are below and far away from the main sequence. *Panels (e), (f), (g), and (h):* histograms of the parallaxes, proper motions, and RVs, respectively.

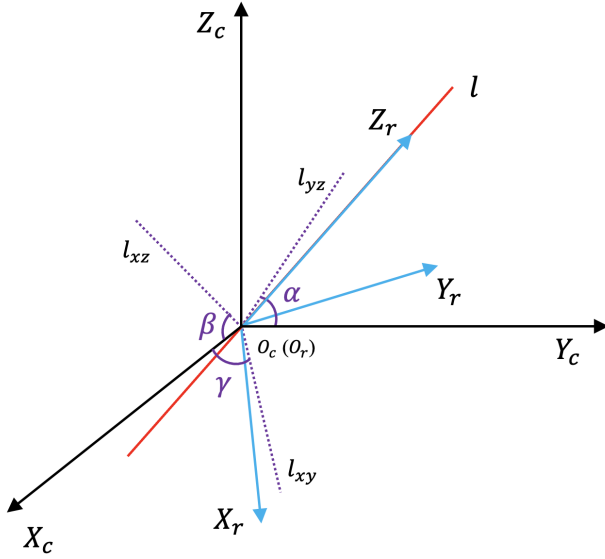
Popov 2020). In total, a sample of 172 member stars of the Praesepe cluster is selected, as listed in Table A1 in the Appendix. If some of the member stars are in binary systems with spurious astrometric solutions, they might affect the kinematics of an OC derived from the astrometric measurements and RVs of the member stars. For the close binary stars, the reliability of astrometry and RVs provided by *Gaia* EDR3 has been improved in comparison with *Gaia* DR2 (Seabroke et al. 2021). As discussed by *Gaia* Collaboration et al. (2021), a value of the parameter `ipd_gof_harmonic_amplitude` above 0.1 in combination with `ruwe` being larger than 1.4 are indicators of a source that is non-single and not correctly handled in the astrometric solution. We do not find such sources in our selected member stars of Praesepe after inspecting these two parameters. For the member stars in the sample, the median uncertainties of the parallax, proper motions  $\mu_{\alpha^*}$  and  $\mu_{\delta}$  are 0.02 mas, 0.02 mas yr<sup>-1</sup>, and 0.015 mas yr<sup>-1</sup>, respectively. The median uncertainty for the RV measurements is 0.9 km s<sup>-1</sup>.

Figure 1 shows the distributions of the astrometric parameters (*RA*, *Dec*,  $\varpi$ ,  $\mu_{\alpha^*}$ ,  $\mu_{\delta}$ , and RVs) of the member stars, including the color-magnitude diagram. It

is shown that the observed parameters of the cluster member stars are approximated by a multidimensional normal distribution.

### 3. METHODS

With the celestial positions, parallaxes, proper motions, and radial velocities given by *Gaia* EDR3, we can determine the 3D spatial coordinates ( $x_g$ ,  $y_g$ ,  $z_g$ ) and the 3D velocity components ( $v_{x_g}$ ,  $v_{y_g}$ ,  $v_{z_g}$ ) of the cluster members (Xu et al. 2013; Reid et al. 2019). The calculations are in the Galactic Cartesian coordinate system ( $O_g$ – $X_gY_gZ_g$ ). The origin of coordinates  $O_g$  is in the Galactic centre. In this step, the distances of sources are derived by inverting the trigonometric parallaxes. The position and velocity uncertainties are estimated with a Monte Carlo method by taking into account the observation errors of astrometric parameters but without considering the covariances between parallaxes and proper motions. At the location of the Sun, the  $X_g$ -axis points to the Galactic centre, the  $Y_g$ -axis towards the direction of the Galactic rotation, and the  $Z_g$ -axis towards the north Galactic pole, respectively. The circular rotation speed at the Sun’s position is adopted as 236



**Figure 2.** Cartesian coordinate system  $O_c-X_c Y_c Z_c$  (black) centered at the OC centre. Also shown is the rotational Cartesian coordinate system  $O_r-X_r Y_r Z_r$  (blue), where  $\vec{l}$  is the rotation axis, in accordance with the  $Z_r$ -axis. The projections of  $\vec{l}$  in the  $Y_c-Z_c$ , the  $X_c-Z_c$ , and the  $X_c-Y_c$  plane are  $l_{yz}$ ,  $l_{xz}$  and  $l_{xy}$ , respectively.  $\alpha$ ,  $\beta$  and  $\gamma$  indicate the included angles between  $l_{yz}$  and the  $Y_c$ -axis,  $l_{xz}$  and the  $X_c$ -axis,  $l_{xy}$  and the  $X_c$ -axis, respectively. The projection of the  $X_r$ -axis in the  $X_c-Y_c$  plane is set to  $l_{xy}$ .

$\pm 7 \text{ km s}^{-1}$ , and the Sun is at a distance of  $8.15 \pm 0.15 \text{ kpc}$  to the Galactic centre (Reid et al. 2019). The three velocity components of the solar motion, i.e., towards the Galactic centre ( $U_\odot$ ), in the direction of Galactic rotation ( $V_\odot$ ), towards the north Galactic North Pole ( $W_\odot$ ), are adopted as  $(U_\odot, V_\odot, W_\odot) = (10.6 \pm 1.2, 10.7 \pm 6.0, 7.6 \pm 0.7) \text{ km s}^{-1}$  (Reid et al. 2019).

By defining the OC centre as the origin of coordinates, a new Cartesian coordinate system  $O_c-X_c Y_c Z_c$  can be established. The OC centre and its uncertainty in the Galactic coordinate system come from the means and standard deviations of the astrometric parameters of the selected member stars by performing the Monte Carlo simulations. The 3D spatial coordinates  $(x_c, y_c, z_c)$  and the 3D velocity components  $(v_{x_c}, v_{y_c}, v_{z_c})$  of a member star in this coordinate system can be calculated as:

$$\begin{pmatrix} x_c \\ y_c \\ z_c \end{pmatrix} = \begin{pmatrix} x_g \\ y_g \\ z_g \end{pmatrix} - \begin{pmatrix} x_{g,s} \\ y_{g,s} \\ z_{g,s} \end{pmatrix}, \quad (1)$$

$$\begin{pmatrix} v_{x_c} \\ v_{y_c} \\ v_{z_c} \end{pmatrix} = \begin{pmatrix} v_{x_g} \\ v_{y_g} \\ v_{z_g} \end{pmatrix} - \begin{pmatrix} v_{x_{g,s}} \\ v_{y_{g,s}} \\ v_{z_{g,s}} \end{pmatrix}, \quad (2)$$

where  $(x_{g,s}, y_{g,s}, z_{g,s})$  are the coordinates of the cluster centre,  $(v_{x_{g,s}}, v_{y_{g,s}}, v_{z_{g,s}})$  represent the 3D systemic velocities of the cluster in the Galactic Cartesian coordinate system. The vectors  $(v_{x_c}, v_{y_c}, v_{z_c})$  are therefore the 3D residual velocities of a member star.

As shown in Figure 2, if a cluster does rotate, the rotation axis  $\vec{l}$  of the cluster in the  $O_c-X_c Y_c Z_c$  system can be determined from the three position angles (PA),  $\alpha$ ,  $\beta$ , and  $\gamma$ . Here, the vector  $\vec{l}$  across the origin  $O_c$  has a positive direction above the  $X_c-Y_c$  plane. Based on the observational data, these angles can be fitted by a residual velocity method adopted in many previous studies (e.g., Bellazzini et al. 2012; Lanzoni et al. 2013; Ferraro et al. 2018; Lanzoni et al. 2018; Loktin & Popov 2020; Leanza et al. 2022). In the following, we describe the procedure to determine the angle  $\alpha$ :

1. The projection of the rotation axis  $\vec{l}$  on the  $Y_c-Z_c$  plane,  $l_{yz}$ , will divide the cluster members into two sub-samples (Figure 2). If the cluster does rotate, the mean residual velocities  $v_{x_c}$  for the member stars of the two different sub-samples should present opposite signs.
2. Starting from the  $Y_c$ -axis ( $\alpha = 0^\circ$ ), the projection of the rotation axis on the  $Y_c-Z_c$  plane,  $l_{yz}$  rotates counterclockwise as the increase of  $\alpha$ . A series of the mean residual velocities  $v_{x_c}$  for the member stars of the two different sub-samples can be calculated. Meanwhile, the Monte Carlo simulations can be preformed to randomly simulate the mean residual velocities and the uncertainties based on the  $v_{x_c}$  values as well as their uncertainties of the member stars.
3. Then, we can determine the dependence of the mean residual velocities on the PA. The mean residual velocity reaches a maximum/minimum at a PA  $\alpha$ , which indicates the projection of the actual rotation axis  $\vec{l}$  of the cluster on the  $Y_c-Z_c$  plane.

Similar methods are used to determine the values of  $\beta$  and  $\gamma$ . As shown in Figure 2,  $\alpha$ ,  $\beta$ , and  $\gamma$  satisfy the relation:  $\tan \alpha \cdot \tan \gamma = \tan \beta$ , which can be used as a test of the three angles calculated by the above method.

Once the rotation axis  $\vec{l}$  of the cluster is determined, we can construct a rotational Cartesian coordinate sys-

**Table 1.** Definitions of the included angle  $\alpha_i$ ,  $\beta_i$  and  $\gamma_i$  between the axes of the Cartesian coordinate system  $O_c-X_cY_cZ_c$  centered at the OC centre and those of the rotational Cartesian coordinate system  $O_r-X_rY_rZ_r$  (also see Figure 2).

	$X_c$ -axis	$Y_c$ -axis	$Z_c$ -axis
$X_r$ -axis	$\alpha_1$	$\beta_1$	$\gamma_1$
$Y_r$ -axis	$\alpha_2$	$\beta_2$	$\gamma_2$
$Z_r$ -axis	$\alpha_3$	$\beta_3$	$\gamma_3$

tem ( $O_r-X_rY_rZ_r$ ) for the cluster, where the origin of coordinates  $O_r$  is located at the cluster centre. The  $Z_r$ -axis is in accordance with the rotation axis  $\vec{l}$ . The projection of the  $X_r$ -axis in the  $X_c-Y_c$  plane is set to be consistent with the projection  $l_{xy}$  of  $\vec{l}$  (Figure 2). Therefore, the vectors of  $X_r$ -axis,  $Y_r$ -axis, and  $Z_r$ -axis in the Cartesian coordinate system  $O_c-X_cY_cZ_c$  can be determined by the angles of  $\alpha$ ,  $\beta$ , and  $\gamma$ , i.e.,

$$\begin{cases} \overrightarrow{O_rX_r} = (1, \tan \gamma, -\frac{1 + \tan^2 \gamma}{\tan \beta}), \\ \overrightarrow{O_rY_r} = (-\tan \gamma, 1, 0), \\ \overrightarrow{O_rZ_r} = (\frac{1}{\tan \beta}, \frac{1}{\tan \alpha}, 1). \end{cases} \quad (3)$$

The 3D coordinates and 3D velocity components in the  $O_c-X_cY_cZ_c$  system are related to those in the  $O_r-X_rY_rZ_r$  system by:

$$\begin{pmatrix} x_r \\ y_r \\ z_r \end{pmatrix} = \begin{pmatrix} \cos \alpha_1 & \cos \beta_1 & \cos \gamma_1 \\ \cos \alpha_2 & \cos \beta_2 & \cos \gamma_2 \\ \cos \alpha_3 & \cos \beta_3 & \cos \gamma_3 \end{pmatrix} \begin{pmatrix} x_c \\ y_c \\ z_c \end{pmatrix}, \quad (4)$$

$$\begin{pmatrix} v_{x_r} \\ v_{y_r} \\ v_{z_r} \end{pmatrix} = \begin{pmatrix} \cos \alpha_1 & \cos \beta_1 & \cos \gamma_1 \\ \cos \alpha_2 & \cos \beta_2 & \cos \gamma_2 \\ \cos \alpha_3 & \cos \beta_3 & \cos \gamma_3 \end{pmatrix} \begin{pmatrix} v_{x_c} \\ v_{y_c} \\ v_{z_c} \end{pmatrix}, \quad (5)$$

here,  $\alpha_i$ ,  $\beta_i$  and  $\gamma_i$  are the included angles listed in Table 1.

The cylindrical coordinate system ( $r, \varphi, z$ ) is more convenient to study the rotational properties of stellar clusters (e.g., Lanzoni et al. 2018), which is adopted in the following analysis. The transformation equations from the Cartesian coordinates to the cylindrical coordinates are:

$$\begin{cases} r = \sqrt{x_r^2 + y_r^2}, \\ \varphi = \text{atan} \frac{y_r}{x_r}, \\ z = z_r. \end{cases} \quad (6)$$

$$\begin{pmatrix} v_r \\ v_\varphi \\ v_z \end{pmatrix} = \begin{pmatrix} \cos \varphi & \sin \varphi & 0 \\ -\sin \varphi & \cos \varphi & 0 \\ 0 & 0 & 1 \end{pmatrix} \begin{pmatrix} v_{x_r} \\ v_{y_r} \\ v_{z_r} \end{pmatrix}. \quad (7)$$

## 4. RESULTS

### 4.1. Rotation in Praesepe

According to the astrometric parameters of the 172 member stars (see Sect. 2), the means and standard deviations of the fundamental parameters of Praesepe are determined as  $(Ra, Dec) = (129.85^\circ \pm 1.51^\circ, 19.52^\circ \pm 1.49^\circ)$ ,  $\varpi = 5.41 \pm 0.20$  mas, proper motions  $(\mu_{\alpha^*}, \mu_\delta) = (-35.82 \pm 1.54, -12.79 \pm 1.09)$  mas yr $^{-1}$ , and  $RV = 35.1 \pm 1.4$  km s $^{-1}$ , which are in good agreement with previous determinations (e.g., Gaia Collaboration et al. 2018a; Röser & Schilbach 2019; Lodieu et al. 2019; Gao 2019; Loktin & Popov 2020). Here, these parameters do not take into account the measurement errors as weights. After applying the Monte Carlo simulation to the means and standard deviations of the parameters from the selected member stars with 3D kinematic measurements, we obtain the centre, systemic motion, and the corresponding uncertainties of Praesepe in the Galactic coordinate system. For each of the member stars, we first calculate its 3D coordinates, 3D velocities, as well as the uncertainties in the Galactic Cartesian coordinate system, then transform them to the  $O_c-X_cY_cZ_c$  system according to Equ. (1) and Equ. (2).

To investigate the rotation and estimate the rotation axis as well as velocity of the Praesepe cluster, we calculate the mean residual velocity of the member stars as a function of the position angle following the method described in Sect. 3. A Monte Carlo method is used to estimate the uncertainties. A step length of  $5^\circ$  for the position angle is adopted in the calculation. The mean residual velocities for the first half of the member stars correspond to the PA from  $5^\circ$  to  $180^\circ$ , and that of the second half correspond to the PA from  $180^\circ$  to  $360^\circ$ . Figure 3(a), (b), and (c) present the mean residual velocity of all the member stars as a function of the PA for  $v_{x_c}$ ,  $v_{y_c}$ , and  $v_{z_c}$ , respectively. The results for those member stars within the tidal radius are shown in Figure 3(d), (e), and (f) for comparison. They all present sinusoidal behaviors, which indicate the rotation of the Praesepe's system. Here the adopted tidal radius of Praesepe is 10 pc. The best-fitting position angles  $\alpha$ ,  $\beta$ , and  $\gamma$  with all the member stars in the sample are  $\alpha = 139.9^\circ \pm 2.9^\circ$ ,  $\beta = 152.2^\circ \pm 6.4^\circ$ , and  $\gamma = 210.2^\circ \pm 1.5^\circ$ , respectively. In comparison, the obtained position angles based on the member stars within the tidal radius are  $\alpha = 120.8^\circ \pm 4.5^\circ$ ,  $\beta = 118.1^\circ \pm 16.5^\circ$ , and  $\gamma = 211.2^\circ$



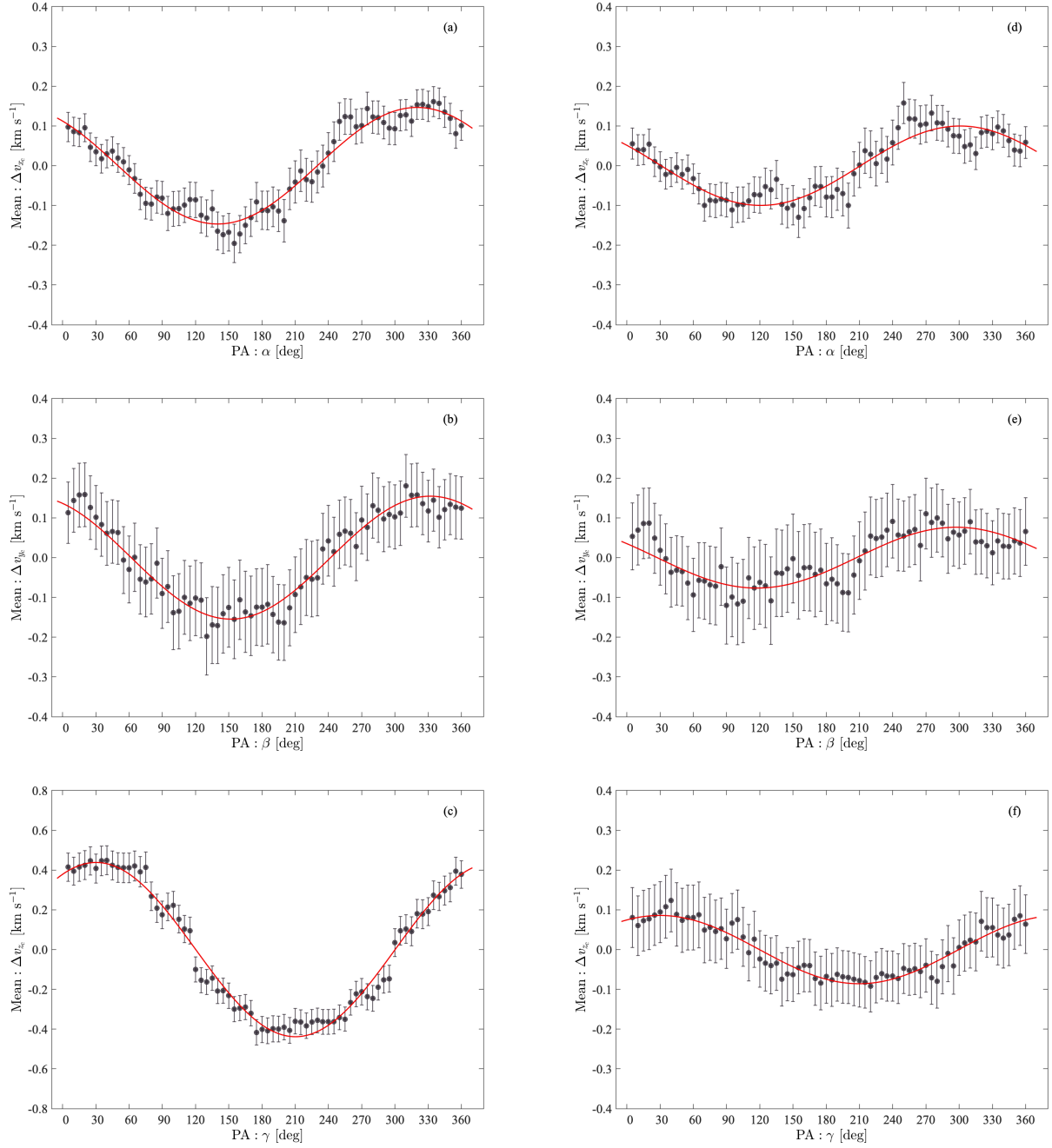


**Figure 3.** Mean residual velocities of  $v_{x_c}$ ,  $v_{y_c}$  and  $v_{z_c}$  as a function of the position angle (PA) are shown in *Panel* (a), (b), and (c), respectively, for all the member stars. The results given in *Panel* (d), (e), and (f) are similar to that of the left column, but derived from the member stars within the tidal radius of Praesepe. The error bars (gray), as well as the best-fitting sine functions (red) are also shown in the plots.

$\pm 7.8^\circ$ , respectively. These fitted position angles satisfy the relation of  $\tan \alpha \cdot \tan \gamma = \tan \beta$  considering the uncertainties.

The member stars beyond the tidal radius are no longer simply controlled by the cluster itself, but influenced by the gravitational force of the Galaxy. Actually, most of the OCs can cross the Galactic plane several times in one orbital period of them (e.g., Wu et al. 2009). Taking this into account, we adopt the best-fitting position angles from the member stars within the cluster tidal radius in the following analysis. Considering the relation of  $\tan \alpha \cdot \tan \gamma = \tan \beta$ , the position angles of  $(\alpha, \beta, \gamma) = (120.8^\circ, 134.5^\circ, 211.2^\circ)$  are adopted in this study to derive the  $(r, \varphi, z)$  and  $(v_r, v_\varphi, v_z)$  of the member stars in the cylindrical coordinate system. The corresponding uncertainties are estimated by a Monte Carlo method. The angle between the rotation axis of the Praesepe cluster and the Galactic plane is estimated to be  $41^\circ \pm 12^\circ$ . Meanwhile, based on the rotational velocities of the member stars, the mean rotational velocity of Praesepe within its tidal radius is estimated to be  $0.2 \pm 0.05 \text{ km s}^{-1}$ , which is concordant with the properties show in Figure 3(d), (e), and (f). Here, the error bar is the uncertainty of the mean rotational velocity, obtained through the Monte Carlo simulation.

Generally, dense molecular cores are the nurseries of embedded clusters, which are predecessors of OCs (e.g., Lada & Lada 2003). Hydrodynamical simulations show that the stellar component of the embedded cluster can inherit the rotation signature from the parent gas and the rotation is common for embedded clusters (Mapelli 2017). The rotation of Praesepe probably originates from the rotational characteristic of its predecessor embedded cluster. From the derived rotational velocities of member stars, it is shown that not all the member stars rotate in the same direction, although this may be partially influenced by the astrometric measurement uncertainties. Such phenomenon also occurs in the rotation of global clusters (e.g., Lanzoni et al. 2018; Leanza et al. 2022). OCs are the survivors of hierarchical or substructured protoclusters that gestated in molecular clouds. Many stellar feedback mechanisms play important roles in the formation of protoclusters, such as protostellar outflows, stellar radiation pressure, stellar winds from massive stars, etc. The mutual interference during stellar cluster formation may result in that not all the member stars of Praesepe neatly rotate in the same direction.

#### 4.2. Rotational properties of stars in Praesepe

Figure 4 shows the rotational velocities  $v_\varphi$  of the cluster members as a function of the distance  $r$  from the cluster centre. A Monte Carlo method is used to esti-

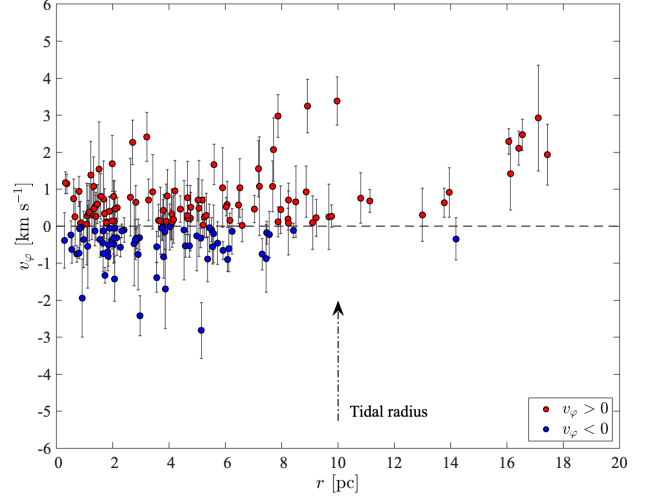


**Figure 4.** The rotational velocity components as a function of the distance  $r$  from the cluster centre, for the cluster members within two times the tidal radius of Praesepe.

mate the uncertainties. The referenced value of the tidal radius of Praesepe is adopted as 10 pc. Inside the tidal radius (10 pc) of the Praesepe cluster, we find that the member stars in the inner region have slightly larger rotational velocities than those in the outer region. Near or beyond the tidal radius of Praesepe, the rotational velocities of the member stars tend to present large dispersion, which may be due to that these stars are partially influenced by the Galactic tidal force, rather than simply dominated by the gravitational force of the cluster itself. Inside the the tidal radius, there are several stars with peculiarly rotational velocities that deviate significantly from the main part, which may be “passing through” stars and not the bona fide members of the Praesepe cluster.

The kinematic property of stars in an OC, e.g., whether the rotation of member stars follow the classical Newton’s theorems, is an interesting question that has not been well addressed. This issue can be explored by comparing the observational results with the theoretical expectations of Newton’s theorems. In the following, we primarily analyze the properties of  $v_\varphi$  of the member stars within the tidal radius of Praesepe. Firstly, assuming that the OC system follows a spherically symmetric density distribution, then the gravitational potential at the radius  $r$  is:

$$\Phi(r) = -4\pi G \left[ \frac{1}{r} \int_0^r \rho(r') r'^2 dr' + \int_r^\infty \rho(r') r' dr' \right]. \quad (8)$$

The asymmetry assumption of the data distribution is evaluated by calculating the skewness of the sample.

The skewness of any perfectly symmetric distribution is zero. If the skewness is between  $-0.50$  and  $0.50$ , the data are suggested to be fairly symmetrical. The Pearson's moment coefficients of skewness of the Galactic longitude, latitude, and parallaxes of all the member stars within the tidal radius of Praesepe are  $0.01$ ,  $-0.13$ , and  $0.11$ , respectively. The results indicate that the stars in the parent catalog described in Sect. 2 present a well spherically symmetric distribution. For the selected 172 member stars with 3D kinematic measurements, the corresponding skewness coefficients are  $0.28$ ,  $-0.35$ , and  $0.15$ , respectively, which are slightly larger than those of the parent sample but still show a good spherically symmetric distribution.

From the Newton's theorems, the gravitational attraction of the system at  $r$  is entirely determined by the mass interior to  $r$ , i.e.,

$$\begin{aligned} \mathbf{F}(r) &= -\frac{d\Phi}{dr} \hat{e}_r = -\frac{GM(r)}{r^2} \hat{e}_r, \\ M(r) &= 4\pi \int_0^r \rho(r') r'^2 dr'. \end{aligned} \quad (9)$$

Here,  $M(r)$  is the mass inside the radius  $r$ ,  $G = 4.3 \times 10^{-3} \text{ pc } M_\odot^{-1} (\text{km s}^{-1})^2$  is the gravitational constant. The circular speed  $v_c(r)$  of the system therefore can be calculated by:

$$v_c^2(r) = r \frac{d\Phi}{dr} = r |\mathbf{F}| = \frac{GM(r)}{r}. \quad (10)$$

Here, this formula is used in an attempt to describe the rotational property of Praesepe, since its rotation has been identified. Although individual stars may not present perfectly circular motion, we can try to make an approximate comparison between the root-mean-square (RMS) rotational velocity derived from cluster members and the theoretical expectation with Equ. (10). Actually, many of the member stars may have residual radial motions as discussed in the next subsection. The same as Röser & Schilbach (2019), the mass density of Praesepe adopted in this study is described by a Plummer model (Plummer 1915), which is:

$$\rho(r) = \frac{3M_t}{4\pi r_{\text{co}}^3} \frac{1}{[1 + (r/r_{\text{co}})^2]^{5/2}}. \quad (11)$$

Here,  $M_t$  is the total mass inside the tidal radius of Praesepe, and  $r_{\text{co}}$  is the core radius. Then,  $M(r)$  and the corresponding circular speed  $v_c(r)$  can be expressed as:

$$M(r) = M_t \cdot \frac{r^3}{(r^2 + r_{\text{co}}^2)^{3/2}}, \quad (12)$$

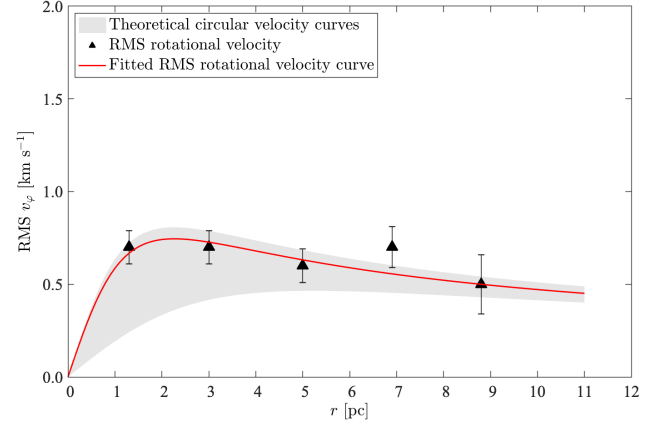


**Figure 5.** Comparison between the observed RMS rotational velocities of the member stars (black triangles) and the theoretical values at distance  $r$  from the cluster centre. The grey shadow shows the theoretical values calculated by Equ. (13) after considering the possible ranges of the tidal mass and the core radius of Praesepe. The red line is a best-fitting curve to the observed RMS rotational velocities.

$$v_c(r) = [GM_t \cdot \frac{r^2}{(r^2 + r_{\text{co}}^2)^{3/2}}]^{1/2}. \quad (13)$$

**Table 2.** RMS rotational velocities of the members stars within the tidal radius of Praesepe, which are derived from the observational data of *Gaia* EDR3.

$R_i$ [pc]	$R_o$ [pc]	$R_m$ [pc]	$N$	RMS $v_\phi$ [km s <sup>-1</sup> ]	$\epsilon_{\text{RMS } v_\phi}$ [km s <sup>-1</sup> ]
(1)	(2)	(3)	(4)	(5)	(6)
0.0	2.0	1.3	46	0.7	0.1
2.0	4.0	3.0	35	0.7	0.1
4.0	6.0	5.0	32	0.6	0.1
6.0	8.0	6.9	19	0.7	0.1
8.0	10.0	8.8	10	0.5	0.2

NOTE—Columns 1–2: the inner and outer radius of each bin; Columns 3–6: the average radius, number of the member stars, RMS rotational velocity and its uncertainty derived from the stars in each bin.

The tidal mass  $M_t$  and the core radius  $r_{\text{co}}$  of Praesepe have been determined by many research works. The estimated value of  $M_t$  is in the range of  $[483, 630] M_\odot$  (e.g., Röser & Schilbach 2019; Wang et al. 2014; Kraus & Hillenbrand 2007; Gao 2019; Adams et al. 2002; Holland et al. 2000). The core radius  $r_{\text{co}}$  is in the range of  $[1.6, 3.7] \text{ pc}$  (e.g., Mermilliod et al. 1990; Adams et al. 2002; Lodieu et al. 2019; Röser & Schilbach 2019; Gao 2019). The difference between the theoretical circular velocities derived from different tidal masses is not very significant, less than  $0.1 \text{ km s}^{-1}$ . While the maximum



difference for the derived core radius is  $\sim 0.3 \text{ km s}^{-1}$ . According to the ranges of  $M_t$  and  $r_{\text{co}}$ , the possible theoretical circular velocity curves are calculated and shown in Figure 5.

For the member stars inside the tidal radius of Praesepe, the median absolute value of their rotational velocities is  $\sim 0.5 \text{ km s}^{-1}$ , and the standard deviation of  $v_\phi$  is  $\sim 1.0 \text{ km s}^{-1}$ . We notice that there are eight stars with  $|v_\phi|$  larger than  $2.0 \text{ km s}^{-1}$ , and deviate from those of the vast majority of the member stars. In order to reduce the influence of the stars with peculiar rotational velocities and investigate the features indicated by vast majority of the member stars, the cluster members with values of  $|v_\phi|$  smaller than  $2.0 \text{ km s}^{-1}$  are extracted from the sample and divided into several bins. Then, we calculate the RMS rotational velocity of the member stars in each bin. The Monte Carlo simulations are used to estimate the uncertainties. The results are shown in Table 2 and Figure 5. The derived RMS rotational velocities are in agreement with the theoretical values. By fitting the RMS velocities listed in Table 2 with Equ. (13), we obtain a core radius of  $1.6 \pm 0.5 \text{ pc}$  and a tidal mass of  $537 \pm 146 M_\odot$  for the Praesepe cluster. The uncertainties are estimated by the Monte Carlo method. The best-fitting RMS velocity curve shown in Figure 5 also indicates that the rotation of member stars within the tidal radius of Praesepe probably follow the Newton's theorems. Besides, according to the best-fitting curve, the member stars at the periphery of the Praesepe cluster may have rotational velocities of about  $0.4 \text{ km s}^{-1}$ .

#### 4.3. Absence of expansion or contraction

During the emerging of an OC from its natal cloud, it can expand for a long period before reaching an equilibrium state (e.g., Kroupa et al. 2001; Lada & Lada 2003; Banerjee & Kroupa 2017). The age of Praesepe is about 590–660 Myr (e.g., Mermilliod 1981; Vandenberg & Bridges 1984; Delorme et al. 2011; Brandt & Huang 2015; Gossage et al. 2018). It is not sure whether the Praesepe cluster is still expanding.

The expansion or contraction of Praesepe can be understood by the statistical analysis on the radial component  $v_r$  of the member stars perpendicular to the rotation axis. Figure 6 shows the radial components of the cluster members within two times the tidal radius (10 pc) of Praesepe as a function of the distance  $r$  from the cluster centre, which does not present a visible indication of expansion or contraction. In addition, the mean radial component  $\bar{v}_r$  of the member stars within 5 pc, 10 pc, and 20 pc of the cluster centre are  $-0.01 \text{ km s}^{-1}$ ,  $0.01 \text{ km s}^{-1}$ , and  $-0.02 \text{ km s}^{-1}$ , with uncertainties of  $0.06 \text{ km s}^{-1}$ ,  $0.05 \text{ km s}^{-1}$ , and  $0.05 \text{ km s}^{-1}$ ,

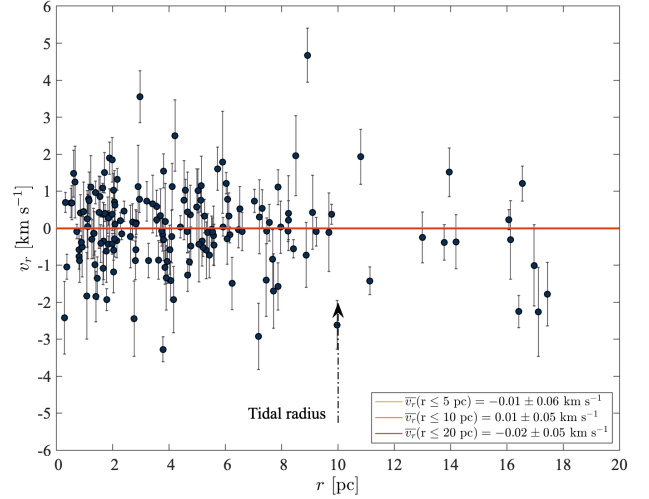


**Figure 6.** The radial velocity components and uncertainties as a function of the distance  $r$  from the cluster centre, for the cluster members within two times the tidal radius of Praesepe. The mean values of the radial components within 5 pc, 10 pc, and 20 pc of the cluster centre all are close to zero, and shown in the panel.

respectively. Here, the error bars are the uncertainties in the mean, obtained through Monte Carlo simulations. The mean radial components are close to zero show that there is no significant indication of expansion or contraction for the Praesepe cluster, implying that the rotation of member stars within the tidal radius of Praesepe can present the closed-loop motion. Figure 6 also implies that there will be a non-negligible radial velocity acceleration and a radial velocity dispersion contribution to the support of the cluster, although the radial velocity dispersion is partially influenced by the astrometric measurement uncertainties. The absence of expansion or contraction of Praesepe suggests that the cluster system should possess additional mass to provide force for supporting the radial velocity acceleration of member stars. It is speculated that the derived dynamic mass in Sect. 4.2 is a lower limit for the Praesepe cluster.

## 5. SUMMARY

In this work, we explored the kinematic properties of Praesepe, the only OC in the Milky Way whose rotation has been investigated exclusively. Based on the high-precision astrometric dataset of *Gaia* EDR3, the rotation in the Praesepe cluster and its rotation axis in the Galaxy were determined by analysing the 3D residual velocities of cluster members for the first time. Our developed methodology also derived the rotational velocity components of the member stars, suggesting that the member stars within the tidal radius of the Praesepe cluster probably also conforms to the theorems of

Newtonian mechanics. Additionally, the current results suggest no significant indication of expansion or contraction for Praesepe.

### ACKNOWLEDGMENTS

We thank the anonymous referee for the instructive comments and suggestions which help us a lot to improve the paper. This work was funded by the NSFC, grant numbers 11933011, 11873019 and 11673066, and by the Key Laboratory for Radio Astronomy. YJL thanks supports from the Natural Science Foundation of Jiangsu Province (grant number BK20210999) and the Entrepreneurship and Innovation Program of Jiangsu Province. LGH thanks the support from the Youth Innovation Promotion Association CAS. We used data from the European Space Agency mission *Gaia* (<http://www.cosmos.esa.int/gaia>), processed by the *Gaia* Data Processing and Analysis Consortium (DPAC; see <http://www.cosmos.esa.int/web/gaia/dpac/consortium>). Funding for DPAC has been provided by national institutions, in particular the institutions participating in the *Gaia* Multilateral Agreement.

### APPENDIX

Table A1 presents the astrometric parameters and errors of examples of selected member stars with 3D kinematic measurements in this work.

### REFERENCES

- Adams, J. D., Stauffer, J. R., Skrutskie, M. F., et al. 2002, *AJ*, 124, 1570, doi: [10.1086/342016](https://doi.org/10.1086/342016)
- Banerjee, S., & Kroupa, P. 2017, *A&A*, 597, A28, doi: [10.1051/0004-6361/201526928](https://doi.org/10.1051/0004-6361/201526928)
- Barnes, S. A. 2007, *ApJ*, 669, 1167, doi: [10.1086/519295](https://doi.org/10.1086/519295)
- Bellazzini, M., Bragaglia, A., Carretta, E., et al. 2012, *A&A*, 538, A18, doi: [10.1051/0004-6361/201118056](https://doi.org/10.1051/0004-6361/201118056)
- Bertelli Motta, C., Salaris, M., Pasquali, A., & Grebel, E. K. 2017, *MNRAS*, 466, 2161, doi: [10.1093/mnras/stw3252](https://doi.org/10.1093/mnras/stw3252)
- Brandt, T. D., & Huang, C. X. 2015, *ApJ*, 807, 24, doi: [10.1088/0004-637X/807/1/24](https://doi.org/10.1088/0004-637X/807/1/24)
- Cantat-Gaudin, T., Jordi, C., Vallenari, A., et al. 2018, *A&A*, 618, A93, doi: [10.1051/0004-6361/201833476](https://doi.org/10.1051/0004-6361/201833476)
- Cantat-Gaudin, T., Anders, F., Castro-Ginard, A., et al. 2020, *A&A*, 640, A1, doi: [10.1051/0004-6361/202038192](https://doi.org/10.1051/0004-6361/202038192)
- Castro-Ginard, A., Jordi, C., Luri, X., et al. 2020, *A&A*, 635, A45, doi: [10.1051/0004-6361/201937386](https://doi.org/10.1051/0004-6361/201937386)
- Castro-Ginard, A., McMillan, P. J., Luri, X., et al. 2021, *A&A*, 652, A162, doi: [10.1051/0004-6361/202039751](https://doi.org/10.1051/0004-6361/202039751)
- Castro-Ginard, A., Jordi, C., Luri, X., et al. 2022, *A&A*, 661, A118, doi: [10.1051/0004-6361/202142568](https://doi.org/10.1051/0004-6361/202142568)
- Delorme, P., Collier Cameron, A., Hebb, L., et al. 2011, *MNRAS*, 413, 2218, doi: [10.1111/j.1365-2966.2011.18299.x](https://doi.org/10.1111/j.1365-2966.2011.18299.x)
- Dias, W. S., Alessi, B. S., Moitinho, A., & Lépine, J. R. D. 2002, *A&A*, 389, 871, doi: [10.1051/0004-6361:20020668](https://doi.org/10.1051/0004-6361:20020668)
- Dobbie, P. D., Pinfield, D. J., Napiwotzki, R., et al. 2004, *MNRAS*, 355, L39, doi: [10.1111/j.1365-2966.2004.08522.x](https://doi.org/10.1111/j.1365-2966.2004.08522.x)
- Dobbie, P. D., Napiwotzki, R., Burleigh, M. R., et al. 2006, *MNRAS*, 369, 383, doi: [10.1111/j.1365-2966.2006.10311.x](https://doi.org/10.1111/j.1365-2966.2006.10311.x)
- Ferraro, F. R., Mucciarelli, A., Lanzoni, B., et al. 2018, *ApJ*, 860, 50, doi: [10.3847/1538-4357/aabe2f](https://doi.org/10.3847/1538-4357/aabe2f)
- Gaia Collaboration, Prusti, T., de Bruijne, J. H. J., et al. 2016, *A&A*, 595, A1, doi: [10.1051/0004-6361/201629272](https://doi.org/10.1051/0004-6361/201629272)

**Table A1.** Astrometric parameters and errors of selected member stars with 3D kinematic measurements.

<i>Gaia</i> ID	$\alpha$ [deg]	$\delta$ [deg]	$l$ [deg]	$b$ [deg]	$\varpi$ [mas]	$\mu_{\alpha^*}$ [mas yr <sup>-1</sup> ]	$\mu_{\delta}$ [mas yr <sup>-1</sup> ]	$G$ [mag]	bp-rp [mag]	$V_r$ [km s <sup>-1</sup> ]
660944717521395840	131.07	18.74	207.34	33.02	5.43 ± 0.02	-35.98 ± 0.02	-11.63 ± 0.02	12.07	1.06	33.66 ± 0.71
660954067666386944	131.32	18.89	207.27	33.30	5.54 ± 0.02	-37.62 ± 0.02	-12.54 ± 0.02	9.52	0.57	34.54 ± 0.54
660957980380034688	130.95	18.80	207.22	32.93	5.40 ± 0.02	-36.14 ± 0.02	-11.78 ± 0.01	9.98	0.64	36.67 ± 1.89
660962863759344768	130.98	18.89	207.12	32.99	5.42 ± 0.02	-36.34 ± 0.02	-12.80 ± 0.01	12.39	1.15	33.96 ± 0.85
660998975844267264	130.20	18.90	206.80	32.30	5.34 ± 0.05	-36.69 ± 0.04	-12.92 ± 0.03	11.27	0.89	35.87 ± 0.40
661004400386393984	130.34	18.93	206.83	32.44	5.40 ± 0.02	-36.58 ± 0.02	-12.45 ± 0.01	12.65	1.22	34.72 ± 0.89
661015915195312512	130.78	19.07	206.85	32.88	5.50 ± 0.05	-36.69 ± 0.05	-12.01 ± 0.04	9.44	0.67	33.15 ± 0.69
661018904492612224	130.93	19.08	206.90	33.01	5.07 ± 0.02	-33.69 ± 0.02	-12.72 ± 0.01	13.04	1.33	37.21 ± 1.18
661028662658249344	130.68	19.10	206.78	32.80	5.57 ± 0.03	-37.39 ± 0.03	-13.66 ± 0.02	11.44	0.92	34.84 ± 0.37
661029384212747392	130.76	19.17	206.73	32.89	5.39 ± 0.02	-36.68 ± 0.02	-11.38 ± 0.02	11.91	1.02	34.00 ± 0.64
661029727808613760	130.67	19.13	206.74	32.80	5.30 ± 0.02	-35.65 ± 0.02	-11.61 ± 0.02	11.92	1.01	35.55 ± 0.57
661031480156796544	130.58	19.15	206.68	32.73	5.36 ± 0.01	-36.07 ± 0.02	-11.65 ± 0.01	13.09	1.40	35.14 ± 1.27
661111538347104512	131.70	19.64	206.56	33.89	5.41 ± 0.02	-36.79 ± 0.02	-12.68 ± 0.01	10.59	0.75	33.59 ± 0.70
661206577385260800	129.99	19.20	206.39	32.23	5.46 ± 0.02	-36.70 ± 0.02	-12.75 ± 0.01	9.38	0.56	35.76 ± 0.42
661207024061875456	129.80	19.12	206.41	32.03	5.42 ± 0.02	-35.45 ± 0.02	-12.26 ± 0.01	10.45	0.73	35.10 ± 0.99
661211727047722752	130.11	19.22	206.42	32.34	5.45 ± 0.02	-36.58 ± 0.03	-11.35 ± 0.02	12.56	1.23	34.96 ± 1.71
661212933936844416	130.11	19.28	206.36	32.36	5.22 ± 0.03	-35.30 ± 0.03	-11.53 ± 0.02	11.01	0.82	33.31 ± 1.07
661216369910684544	130.03	19.31	206.29	32.29	5.44 ± 0.04	-36.05 ± 0.04	-11.89 ± 0.03	10.81	0.93	36.81 ± 1.09
661221764391246080	130.44	19.27	206.50	32.65	5.59 ± 0.02	-36.92 ± 0.02	-12.99 ± 0.02	10.05	0.67	35.13 ± 0.31
661222279785743616	130.55	19.28	206.53	32.74	5.44 ± 0.02	-36.82 ± 0.02	-12.38 ± 0.01	11.93	1.03	34.29 ± 0.47
661234473194513664	130.45	19.46	206.29	32.72	5.62 ± 0.05	-38.55 ± 0.06	-10.85 ± 0.04	13.22	1.46	37.46 ± 1.35
661235989321322240	130.67	19.54	206.28	32.94	5.37 ± 0.02	-36.98 ± 0.02	-12.38 ± 0.01	9.67	0.59	36.12 ± 1.88
661239390935360512	130.28	19.45	206.23	32.57	5.51 ± 0.02	-38.02 ± 0.02	-12.07 ± 0.01	12.17	1.09	35.39 ± 0.79
661242895630246016	130.22	19.48	206.17	32.53	5.38 ± 0.02	-35.34 ± 0.02	-12.31 ± 0.02	10.18	0.67	34.43 ± 0.32
661243273585807872	130.09	19.46	206.14	32.41	5.41 ± 0.02	-35.37 ± 0.02	-12.81 ± 0.02	10.54	0.74	36.76 ± 0.49
...										

NOTE—The full table is available online.

Gaia Collaboration, Babusiaux, C., van Leeuwen, F., et al. 2018a, *A&A*, 616, A10, doi: [10.1051/0004-6361/201832843](https://doi.org/10.1051/0004-6361/201832843)

Gaia Collaboration, Brown, A. G. A., Vallenari, A., et al. 2018b, *A&A*, 616, A1, doi: [10.1051/0004-6361/201833051](https://doi.org/10.1051/0004-6361/201833051)

—. 2021, *A&A*, 649, A1, doi: [10.1051/0004-6361/202039657](https://doi.org/10.1051/0004-6361/202039657)

Gao, X.-h. 2019, *MNRAS*, 486, 5405, doi: [10.1093/mnras/stz1213](https://doi.org/10.1093/mnras/stz1213)

Gossage, S., Conroy, C., Dotter, A., et al. 2018, *ApJ*, 863, 67, doi: [10.3847/1538-4357/aad0a0](https://doi.org/10.3847/1538-4357/aad0a0)

Gunn, J. E., Griffin, R. F., Griffin, R. E. M., & Zimmerman, B. A. 1988, *AJ*, 96, 198, doi: [10.1086/114801](https://doi.org/10.1086/114801)

Hanson, R. B. 1975, *AJ*, 80, 379, doi: [10.1086/111753](https://doi.org/10.1086/111753)

Hao, C. J., Xu, Y., Wu, Z. Y., et al. 2022, *A&A*, 660, A4, doi: [10.1051/0004-6361/202243091](https://doi.org/10.1051/0004-6361/202243091)

Hao, C. J., Xu, Y., Hou, L. G., et al. 2021, *A&A*, 652, A102, doi: [10.1051/0004-6361/202140608](https://doi.org/10.1051/0004-6361/202140608)

Healy, B. F., McCullough, P. R., & Schlaufman, K. C. 2021, *ApJ*, 923, 23, doi: [10.3847/1538-4357/ac281d](https://doi.org/10.3847/1538-4357/ac281d)

Holland, K., Jameson, R. F., Hodgkin, S., Davies, M. B., & Pinfield, D. 2000, *MNRAS*, 319, 956, doi: [10.1046/j.1365-8711.2000.03949.x](https://doi.org/10.1046/j.1365-8711.2000.03949.x)

Hou, L. G. 2021, *FrASS*, 8, 103, doi: [10.3389/fspas.2021.671670](https://doi.org/10.3389/fspas.2021.671670)

Kamann, S., Bastian, N. J., Giesles, M., Balbinot, E., & Hénault-Brunet, V. 2019, *MNRAS*, 483, 2197, doi: [10.1093/mnras/sty3144](https://doi.org/10.1093/mnras/sty3144)

Khalaj, P., & Baumgardt, H. 2013, *MNRAS*, 434, 3236, doi: [10.1093/mnras/stt1239](https://doi.org/10.1093/mnras/stt1239)

Kharchenko, N. V., Piskunov, A. E., Schilbach, E., Röser, S., & Scholz, R. D. 2013, *A&A*, 558, A53, doi: [10.1051/0004-6361/201322302](https://doi.org/10.1051/0004-6361/201322302)

Klein Wassink, W. J. 1924, *BAN*, 2, 183

—. 1927, *PGro*, 41, 1

Kraus, A. L., & Hillenbrand, L. A. 2007, *AJ*, 134, 2340, doi: [10.1086/522831](https://doi.org/10.1086/522831)

Kroupa, P., Aarseth, S., & Hurley, J. 2001, *MNRAS*, 321, 699, doi: [10.1046/j.1365-8711.2001.04050.x](https://doi.org/10.1046/j.1365-8711.2001.04050.x)

Lada, C. J., & Lada, E. A. 2003, *ARA&A*, 41, 57, doi: [10.1146/annurev.astro.41.011802.094844](https://doi.org/10.1146/annurev.astro.41.011802.094844)

Lanzoni, B., Mucciarelli, A., Origlia, L., et al. 2013, *ApJ*, 769, 107, doi: [10.1088/0004-637X/769/2/107](https://doi.org/10.1088/0004-637X/769/2/107)

Lanzoni, B., Ferraro, F. R., Mucciarelli, A., et al. 2018, *ApJ*, 861, 16, doi: [10.3847/1538-4357/aac26a](https://doi.org/10.3847/1538-4357/aac26a)

- Leanza, S., Pallanca, C., Ferraro, F. R., et al. 2022, *ApJ*, 929, 186, doi: [10.3847/1538-4357/ac5d4e](https://doi.org/10.3847/1538-4357/ac5d4e)
- Lodieu, N., Pérez-Garrido, A., Smart, R. L., & Silvotti, R. 2019, *A&A*, 628, A66, doi: [10.1051/0004-6361/201935533](https://doi.org/10.1051/0004-6361/201935533)
- Loktin, A. V., & Popov, A. A. 2020, *AN*, 341, 638, doi: [10.1002/asna.202013687](https://doi.org/10.1002/asna.202013687)
- Mapelli, M. 2017, *MNRAS*, 467, 3255, doi: [10.1093/mnras/stx304](https://doi.org/10.1093/mnras/stx304)
- Marino, A. F., Milone, A. P., Casagrande, L., et al. 2018, *ApJL*, 863, L33, doi: [10.3847/2041-8213/aad868](https://doi.org/10.3847/2041-8213/aad868)
- Mermilliod, J. C. 1981, *A&A*, 97, 235
- Mermilliod, J. C., Weis, E. W., Duquennoy, A., & Mayor, M. 1990, *A&A*, 235, 114
- Perryman, M. A. C., Brown, A. G. A., Lebreton, Y., et al. 1998, *A&A*, 331, 81, <https://arxiv.org/abs/astro-ph/9707253>
- Pinsonneault, M. H., Stauffer, J., Soderblom, D. R., King, J. R., & Hanson, R. B. 1998, *ApJ*, 504, 170, doi: [10.1086/306077](https://doi.org/10.1086/306077)
- Plummer, H. C. 1915, *MNRAS*, 76, 107, doi: [10.1093/mnras/76.2.107](https://doi.org/10.1093/mnras/76.2.107)
- Poggio, E., Drimmel, R., Cantat-Gaudin, T., et al. 2021, *A&A*, 651, A104, doi: [10.1051/0004-6361/202140687](https://doi.org/10.1051/0004-6361/202140687)
- Reid, M. J., Menten, K. M., Brunthaler, A., et al. 2019, *ApJ*, 885, 131, doi: [10.3847/1538-4357/ab4a11](https://doi.org/10.3847/1538-4357/ab4a11)
- Röser, S., & Schilbach, E. 2019, *A&A*, 627, A4, doi: [10.1051/0004-6361/201935502](https://doi.org/10.1051/0004-6361/201935502)
- Seabroke, G. M., Fabricius, C., Teyssier, D., et al. 2021, *A&A*, 653, A160, doi: [10.1051/0004-6361/202141008](https://doi.org/10.1051/0004-6361/202141008)
- Vandenberg, D. A., & Bridges, T. J. 1984, *ApJ*, 278, 679, doi: [10.1086/161836](https://doi.org/10.1086/161836)
- Vereshchagin, S. V., & Chupina, N. V. 2013, *AN*, 334, 892, doi: [10.1002/asna.201311938](https://doi.org/10.1002/asna.201311938)
- Vereshchagin, S. V., Reva, V. G., & Chupina, N. V. 2013, *ARep*, 57, 52, doi: [10.1134/S1063772912120062](https://doi.org/10.1134/S1063772912120062)
- Wang, P. F., Chen, W. P., Lin, C. C., et al. 2014, *ApJ*, 784, 57, doi: [10.1088/0004-637X/784/1/57](https://doi.org/10.1088/0004-637X/784/1/57)
- Wayman, P. A. 1967, *PASP*, 79, 156, doi: [10.1086/128457](https://doi.org/10.1086/128457)
- Wu, Z.-Y., Zhou, X., Ma, J., & Du, C.-H. 2009, *MNRAS*, 399, 2146, doi: [10.1111/j.1365-2966.2009.15416.x](https://doi.org/10.1111/j.1365-2966.2009.15416.x)
- Xu, Y., Li, J. J., Reid, M. J., et al. 2013, *ApJ*, 769, 15, doi: [10.1088/0004-637X/769/1/15](https://doi.org/10.1088/0004-637X/769/1/15)